Pulay forces from localized orbitals optimized in situ using a psinc basis set

Álvaro Ruiz-Serrano, Nicholas D. M. Hine, and Chris-Kriton Skylaris

Citation: J. Chem. Phys. **136**, 234101 (2012); doi: 10.1063/1.4728026
View online: http://dx.doi.org/10.1063/1.4728026
View Table of Contents: http://jcp.aip.org/resource/1/JCPSA6/v136/i23
Published by the American Institute of Physics.

Pulay forces from localized orbitals optimized *in situ* using a psinc basis set

Álvaro Ruiz-Serrano,[1] Nicholas D. M. Hine,[2] and Chris-Kriton Skylaris[1,a)]
[1]*School of Chemistry, University of Southampton, Highfield, Southampton SO17 1BJ, United Kingdom*
[2]*Department of Physics and Department of Materials, Imperial College London, Exhibition Road, London SW7 2AZ, United Kingdom*

(Received 16 April 2012; accepted 24 May 2012; published online 15 June 2012)

In situ optimization of a set of localized orbitals with respect to a systematically improvable basis set independent of the position of the atoms, such as psinc functions, would theoretically eliminate the correction due to Pulay forces from the total ionic forces. We demonstrate that for strict localization constraints, especially with small localization regions, there can be non-negligible Pulay forces that must be calculated as a correction to the Hellmann-Feynman forces in the ground state. Geometry optimization calculations, which rely heavily upon accurate evaluation of the total ionic forces, show much better convergence when Pulay forces are included. The more conventional case, where the local orbitals remain fixed to pseudo-atomic orbital multiple-ζ basis sets, also benefits from this implementation. We have validated the method on several test cases, including a DNA fragment with 1045 atoms. © *2012 American Institute of Physics*. [http://dx.doi.org/10.1063/1.4728026]

I. INTRODUCTION

Kohn-Sham density functional theory (DFT)[1,2] is widely used to determine properties of materials and molecules at the level of quantum theory. The computational cost of traditional approaches to DFT (Refs. 3–7) scales as $\mathcal{O}(N^3)$, where N is the number of atoms in the system, usually limiting the range of calculations to no more than some hundreds of atoms. More recently, efforts have been put in the development of linear-scaling approaches based on the principle of *nearsightedness* of electronic matter.[8] In systems with a non-zero band gap, the single-particle density matrix decays exponentially with the distance between two points. This property can be exploited to reduce the computational cost to $\mathcal{O}(N)$ by introducing spatially localized orbitals and by truncating the elements of the density matrix that belong to atoms further than a given cutoff radius.[9,10] Programs such as ONETEP,[11] CONQUEST,[12] SIESTA,[13] and OPENMX[14] belong to this category of linear-scaling methods and are capable to perform calculations on thousands of atoms.[15]

The ground state is found by self-consistent field (SCF) minimization of the energy with respect to a number of variational parameters of the system.[16] The Hellmann-Feynman (HF) theorem[17,18] provides a computationally efficient method for calculating the ionic forces at the ground state of the system that eliminates the need to calculate the derivatives of the variational parameters that describe the orbitals. The Hellmann-Feynman theorem holds for self-consistent solutions in the limit of a complete basis set.[19–21] However, practical computational approaches to DFT employ a finite number of basis set functions with a certain degree of incompleteness. In such cases, Pulay forces[22] must be calculated as corrections to the Hellmann-Feynman forces if the basis set functions explicitly depend on the ionic positions. Other approaches[23] perform a self-consistent optimization of the center of localization of the orbitals, so that the Pulay forces vanish at the ground state.

Different choices of localized atomic orbitals include analytical functions such as Gaussian[24,25] or Slater-type[26] orbitals and numerical representations such as all-electron numerical atomic orbitals[27,28] or pseudo-atomic orbitals (PAOs)[29–33] to account for the valence electrons. Schemes using a combination of plane waves and Gaussian localized orbitals have also been developed.[34–37]

The quality of the basis set is controlled by the number of functions for each atomic shell and the symmetry inherent to the angular momentum of each of these functions. These factors are used to construct multiple-ζ basis sets, which can also contain polarization and diffuse orbitals, key to describing the electronic structure of a molecular system. A large number of basis functions is normally required to achieve chemical accuracy in the description of the Kohn-Sham ground state. To reduce the number of atomic orbitals without decreasing the accuracy, a set containing the minimum number of localized orbitals to describe the valence electrons can be optimized *in situ* in terms of a systematically improvable basis set.[38] This maneuver removes the restriction of fixed angular shape characteristic of conventional atomic orbitals.

In this work, we show that Pulay forces must be calculated in cases where the localized orbitals are optimized in terms of a basis set independent of the ionic coordinates. Geometry optimizations carried out with corrected forces show improved systematic convergence with the basis set, allowing efficient calculations on complex molecules. Additionally, Pulay forces are necessary in the more conventional case where the localized orbitals remain fixed in the shape of atomic orbitals. In some cases, especially for large systems, geometry optimization calculations with fixed multiple-ζ PAO basis set can result in faster time-to-solution runtimes, whilst retaining high accuracy in the final geometries.

a)Electronic mail: C.Skylaris@soton.ac.uk.

We have implemented the functionality that enables calculation of Pulay forces within the ONETEP[11] program. Section II offers a brief description of the SCF minimization of the energy and explains the conditions that must be met at convergence of the calculations. In Sec. III, we elaborate on the evaluation of the ionic forces and the origin of the Pulay forces as a consequence of the strict localization constraints. In Sec. IV, we show our results regarding the convergence of the total forces in ONETEP, including the Pulay forces, with respect to the basis set for a CO_2 molecule and a water dimer complex. We then demonstrate that the Pulay terms do not vanish when the localized orbitals are optimized *in situ* with respect to a position-independent basis set. To validate our method, we performed geometry optimization calculations on an adenine-thymine DNA base pair, and on the self-assembling superstructure known as the "tennis-ball" dimer.[39,40] To demonstrate the applicability of our methods to large-scale systems, we performed geometry optimization calculations on a DNA fragment of 1045 atoms, and we provide an example of time saving when using a PAO multiple-ζ basis set of medium size.

II. ENERGY MINIMIZATION

ONETEP[11] is based on a reformulation of Kohn-Sham DFT with norm-conserving pseudopotentials[41,42] in terms of the single-particle density matrix, $\rho(\mathbf{r}, \mathbf{r}')$, expressed in terms of a set of non-orthogonal generalized Wannier functions (NGWFs),[43] $\phi_\alpha(\mathbf{r})$, as:

$$\rho(\mathbf{r}, \mathbf{r}') = \phi_\alpha(\mathbf{r}) K^{\alpha\beta} \phi^*_\beta(\mathbf{r}'), \tag{1}$$

where our notation assumes implicit summation over repeated Greek indexes. The matrix elements $K^{\alpha\beta}$ form the density kernel. In non-metallic systems, $K^{\alpha\beta}$ are non-zero only if $|\mathbf{R}_\alpha - \mathbf{R}_\beta| < R_K$, with $\mathbf{R}_\alpha$ and $\mathbf{R}_\beta$ being the coordinates of the centers of the NGWFs α and β, and R_K a real-space cutoff length.[44]

The NGWFs are non-orthogonal functions centered on the nuclear coordinates which are enforced to be strictly localized within a sphere of finite radius R_α. The overlap matrix $\mathbf{S}$ is defined as,

$$S_{\alpha\beta} = \int d\mathbf{r}\, \phi_\alpha(\mathbf{r}) \phi^*_\beta(\mathbf{r}). \tag{2}$$

At the same time, the NGWFs are expanded as a linear combination of psinc functions,[45] $D_m(\mathbf{r})$, as,

$$\phi_\alpha(\mathbf{r}) = \sum_{m}^{m \in LR(\alpha)} D(\mathbf{r} - \mathbf{r}_m) c_{m\alpha}, \tag{3}$$

where the m index denotes the points of the real-space Cartesian grid $\mathbf{r}_m$ inside the localization region of ϕ_α, referred to as $LR(\alpha)$. The psinc functions form an orthogonal basis set of bandwidth-limited delta functions related to plane-waves by a unitary transformation. Hence, they share many of their desirable properties, notably, the independence from the nuclear coordinates and the ability to form a basis set that can be systematically improved by increasing a single parameter: the kinetic energy cutoff.[42]

The total energy is minimized self-consistently with respect to $K^{\alpha\beta}$ and $c_{m\alpha}$ in two nested loops,[43,46] subject to the constraints of conservation of the total number of electrons and idempotency of the density kernel. The first constraint is enforced by ensuring that the density kernel is appropriately scaled so that the relation $tr[\mathbf{KS}] = N_e$ holds at all points during the energy minimization. On the other hand, idempotency is taken into account by using the Li-Nunes-Vanderbilt (LNV) method,[47] which builds an idempotent density kernel $\mathbf{K}$ from a nearly idempotent matrix $\mathbf{L}$ whose elements are found by direct energy minimization. This scheme also preserves the orthonormality of the Kohn-Sham states at zero electronic temperature. As a result, the converged, self-consistent solution satisfies,

$$\frac{\partial E}{\partial K^{\alpha\beta}} = 0 \ \forall\ \alpha, \beta, \tag{4}$$

and

$$\frac{\delta E}{\delta \phi_\alpha} = 0 \ \forall\ \alpha. \tag{5}$$

We emphasize that the NGWFs are optimized *in situ* based on the variational principle. The condition in Eq. (5) expresses the fact that at self-consistency the energy is stationary with respect to the NGWFs represented as a linear combination of psinc functions. Therefore, at self-consistency, the following condition is also true:

$$\frac{\delta E}{\delta c_{m\alpha}} = 0 \ \forall\ m, \alpha. \tag{6}$$

An alternative approach to self-consistent energy minimization is to employ a single loop to optimize the elements of the density kernel. In these cases, the basis set is formed by localized orbitals which remain fixed during the calculation. A recent addition to ONETEP allows generation of suitable multiple-ζ basis sets out of PAOs that can be used to obtain accurate results given a large enough basis. The PAOs are closely related to the Sankley-Niklewski "fireballs"[29] subject to strict localization constraints. The PAO solver is described in the Appendix. The NGWFs differ from the PAOs in that they are expressed and optimized *in situ* in terms of a linear combination of psinc basis functions. The PAOs, although they are also expressed in terms of psincs for consistency throughout, remain fixed during the calculation. Consequently, the condition in Eq. (5) never holds for PAOs.

III. IONIC FORCES

The evaluation of the ionic forces using NGWFs in ONETEP has been studied previously in Ref. 48. The force acting on ion γ is defined as the negative total derivative of the energy with respect to the nuclear coordinates,

$$\mathbf{F}_\gamma = -\frac{dE}{d\mathbf{R}_\gamma} = -\frac{\partial E}{\partial \mathbf{R}_\gamma} - \frac{\partial E}{\partial K^{\beta\alpha}} \frac{\partial K^{\alpha\beta}}{\partial \mathbf{R}_\gamma} - \int d\mathbf{r} \frac{\delta E}{\delta \phi_\alpha(\mathbf{r})} \frac{\partial \phi_\alpha(\mathbf{r})}{\partial \mathbf{R}_\gamma}. \tag{7}$$

This equation includes terms due to the *explicit* dependency of the energy on the nuclear coordinates, and terms due to the *implicit* dependency of the density kernel and NGWFs on the nuclear coordinates.

When self-consistent convergence is achieved, the conditions in Eqs. (4) and (5) apply, leaving a much simpler expression for the total force,

$$\mathbf{F}_\gamma = -\frac{\partial E}{\partial \mathbf{R}_\gamma}. \tag{8}$$

This result corresponds to direct application of the Hellmann-Feynman theorem after successful SCF energy minimization, with vanishing Pulay forces. The total Hellmann-Feynman force on atom γ is formed by individual contributions to the Hamiltonian, and does not consider derivatives of the NGWFs. In this case, the terms included in the total force are those due to the local and non-local terms of the pseudopotential, the Ewald energy, and (where applicable) non-linear core correction (NLCC) terms,

$$\mathbf{F}_\gamma^{\mathrm{HF}} = \mathbf{F}_\gamma^{\mathrm{nl}} + \mathbf{F}_\gamma^{\mathrm{loc}} + \mathbf{F}_\gamma^{\mathrm{ew}} + \mathbf{F}_\gamma^{\mathrm{NLCC}}. \tag{9}$$

The ionic forces calculated using this expression are generally valid in all cases where both the density kernel and the localized orbitals are optimized to self-consistency.[48]

The LNV algorithm[46,47] allows to converge the energy with respect to $K^{\alpha\beta}$ to a very tight tolerance, so that the condition in Eq. (4) is regularly achieved. However, in many cases, obtaining tight convergence of energy with respect to the psinc expansion of the NGWFs can be very difficult. The competing effects of the kinetic energy operator, which tends to spread the NGWFs across the cell, and the constraint of strict localization within a sphere can result in the NGWF energy gradient converging to small non-zero values.[49] Whereas the total energy converges quadratically with respect to the Kohn-Sham states during the SCF procedure, the forces converge at a slower rate.[22] As a result, the residual NGWF energy gradient has a negligible effect in the evaluation of the ground-state energy, yet can produce non-negligible corrections to the Hellmann-Feynman forces. The Pulay forces in ONETEP are due entirely to the NGWF gradient contribution in Eq. (7),

$$\mathbf{F}_\gamma^{\mathrm{Pulay}} = \int d\mathbf{r} \frac{\delta E}{\delta \phi_\alpha(\mathbf{r})} \frac{\partial \phi_\alpha(\mathbf{r})}{\partial \mathbf{R}_\gamma}. \tag{10}$$

Therefore, given convergence of the energy with respect to the density kernel and the NGWFs, the total force on atom γ is the sum of the Hellmann-Feynman and Pulay forces, $\mathbf{F}_\gamma^{\mathrm{total}} = \mathbf{F}_\gamma^{\mathrm{HF}} + \mathbf{F}_\gamma^{\mathrm{Pulay}}$.

This expression is valid for any set of localized functions. As the PAOs are also represented as a linear combination of psinc functions, the method presented hereafter for determining the Pulay forces holds for both NGWFs and PAOs. As seen from Eq. (10), the Pulay forces require the evaluation of two terms and the integration of their product on a real space grid within the localization region of the relevant NGWF. These terms are the energy gradient with respect to the NGWFs and the derivative of the NGWFs with respect to the ionic coordinates. The first is evaluated at each step of the SCF optimization of the NGWFs and does not need to be re-calculated to evaluate the forces. This makes the computation of Pulay forces inexpensive compared to the SCF cycle, which takes most of the computational effort. The analytical form of $\frac{\delta E}{\delta \phi_\alpha(\mathbf{r})}$ has been derived before by Soler *et al.*[13] for a generalized Lagrangian to keep orthonormality of the Kohn-Sham states and by Miyazaki *et al.*[50] for the LNV method. The expression is equivalent in the case of ONETEP,

$$\frac{\delta E}{\delta \phi_\alpha(\mathbf{r})} = 4[\hat{H}\phi_\beta(\mathbf{r})K^{\beta\alpha} + \phi_\beta(\mathbf{r})Q^{\beta\alpha}], \tag{11}$$

where, for a converged density kernel, $Q^{\alpha\beta} = -(KHS^{-1})^{\alpha\beta}$. The prefactor of 4 in Eq. (11) appears as the NGWFs are real functions and closed shells are assumed.

On the other hand, derivatives with respect to the ionic coordinates can be calculated by applying the gradient operator, $\nabla_{\mathbf{r}}$, to the NGWFs,

$$\frac{\partial \phi_\alpha(\mathbf{r})}{\partial \mathbf{R}_\gamma} = -\nabla_{\mathbf{r}}\phi_\alpha(\mathbf{r})\delta_{\alpha\gamma}. \tag{12}$$

This operation takes places in the reciprocal space representation of the function $\phi_\alpha(\mathbf{r})$ using the well-tested FFT-box technique.[45] The equivalence of the psinc functions and plane waves allows us to expand Eq. (3) as,

$$\phi_\alpha(\mathbf{r}) = \frac{1}{N_p}\sum_{\mathbf{G}}^{\mathbf{G}_{\max}} \tilde{\phi}_\alpha(\mathbf{G}) e^{i\mathbf{G}(\mathbf{r}-\mathbf{R}_\alpha)}, \tag{13}$$

where $\mathbf{G}$ denotes the reciprocal lattice vectors on the FFT-box up to a magnitude of $\mathbf{G}_{\max}$, defined by the kinetic energy cutoff. N_p indicates the number of points in the FFT-box, whose size is proportional to the NGWF radii. It is necessary to stress that the dependency of $\phi_\alpha(\mathbf{r})$ on $\mathbf{R}_\alpha$ does not involve a change in the functional form of the NGWFs as expressed in terms of the psinc basis set, but instead it remains as a translational phase factor that takes into account the displacement of the NGWF center across the simulation cell. Direct differentiation of Eq. (13) provides the derivative of the NGWFs with respect to $\mathbf{R}_\gamma$,

$$\frac{\partial \phi_\alpha(\mathbf{r})}{\partial \mathbf{R}_\gamma} = \frac{1}{N_p}\sum_{\mathbf{G}}^{\mathbf{G}_{\max}} -i\mathbf{G}\tilde{\phi}_\alpha(\mathbf{G}) e^{i\mathbf{G}(\mathbf{r}-\mathbf{R}_\alpha)}\delta_{\alpha\gamma}. \tag{14}$$

Equations (11) and (14) are evaluated in the FFT-box of ϕ_α, so that $\mathbf{F}_\gamma^{\mathrm{Pulay}}$ can be calculated with $\mathcal{O}(N)$ cost.

IV. RESULTS

A. Convergence of the forces

Convergence with respect to the psinc basis set, determined by the kinetic energy cutoff, and the radius of the spherical localization region of the NGWFs, is vital for accurate calculation of ionic forces within this method. This aspect has been studied in Ref. 48 for the Hellmann-Feynman forces alone. Figure 1 reproduces some of the results present in that work and additionally demonstrates the effect of the Pulay correction to the total forces. The calculations involve the force acting on an oxygen atom in CO_2 and the force acting on a hydrogen atom in a H_2O dimer. We used the local-density approximation (LDA) exchange-correlation

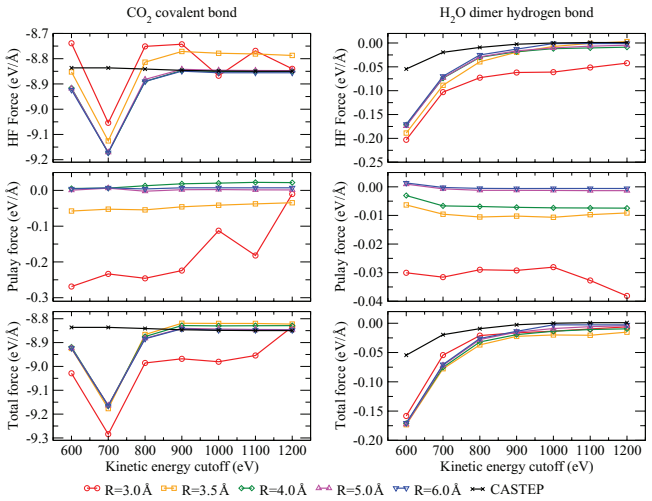

FIG. 1. Convergence of the forces with respect to the kinetic energy cutoff and the NGWF radius. Left: force acting on an oxygen atom in CO_2 along the covalent bond. Right: force acting on a hydrogen atom in H_2O dimer along the hydrogen bond. The first row corresponds to the Hellmann-Feynman force, the second to the Pulay force, and the third are the Pulay-corrected (PC) total forces (Hellmann-Feynman forces plus Pulay). *R* refers to the NGWF radii.

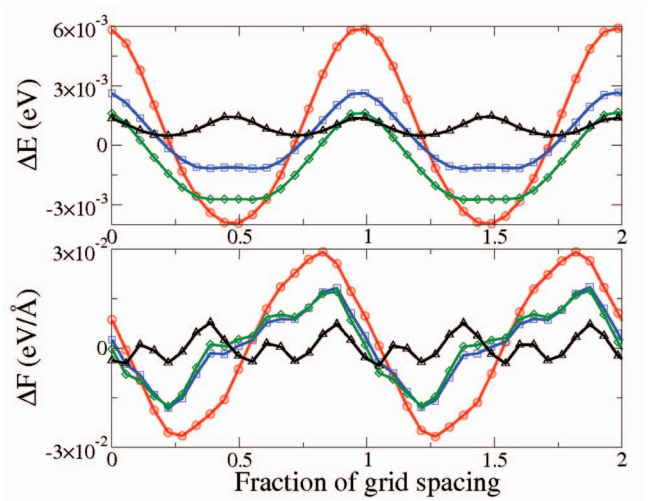

FIG. 2. Egg-box effect on the energy (top) and force along the covalent bond (bottom) of a CO_2 molecule with SZ (red circles), DZP (blue squares), and TZDP (green diamonds) PAO basis sets and NGWFs (black triangles).

functional and employed one NGWF for hydrogen and four for carbon and oxygen atoms.

The total forces, calculated as the sum of the Hellmann-Feynman components and the Pulay corrections, converge to a single value as the kinetic energy cutoff and the NGWF radii increase, and are comparable to the results obtained with traditional plane-wave DFT using CASTEP. The Pulay corrections to the Hellmann-Feynman forces ensure a greater degree of consistency between ground-state energies and the total force acting on ions for any size of localization region. The Pulay forces take a non-negligible value for small localization radii, and converge to zero when the NGWFs become larger and more delocalized. Also, they do not vanish as the kinetic energy cutoff increases, showing the strong correlation with the localization constraint. The relative strength of the Pulay correction is greater in the case of the hydrogen bond in the water dimer (up to 15% of the Hellmann-Feynman force) than in the covalent bond of CO_2 (3%). Therefore, Pulay forces can be expected to play a more significant role in the ionic forces of weakly bonded systems, particularly when modeled with small NGWF radii.

Real-space grid methods can suffer from the so-called "egg-box" effect,[51,52] which appears when the localized orbitals are displaced by a fraction of the grid-spacing in the simulation cell, generating periodic oscillations of the converged ground-state energy and forces. An estimation of the egg-box effect in the total energy and the forces is shown in Fig. 2. These calculations consecutively displace a CO_2 molecule along the first axis of the simulation cell (parallel to the CO_2 covalent bond) by a given step of 1/20 of the grid spacing of 0.24 Å. We use the Perdew-Burke-Ernzerhof (PBE) exchange-correlation functional[53] with a kinetic energy cutoff of 1000 eV and NGWF radii of 4.23 Å to ensure convergence of the forces with the basis set. Single-zeta (SZ), double-zeta plus polarization (DZP), and TZDP basis sets were constructed using PAOs as described in the Appendix. The magnitude of the egg-box effect is reduced when NGWFs are used instead of PAOs contributing to more stability in calculations where the ionic coordinates vary, such as geometry optimization. The maximum variation of the energy using NGWFs is of 1.6×10^{-3} eV, which is up to ten times smaller compared to SZ calculations. NGWFs also reduce the magnitude of the egg-box effect on the forces to 0.01 eV/Å, nearly a third of the magnitude in the case of SZ calculations.

B. Geometry optimization using NGWFs

We have performed geometry optimization calculations using the Broyden-Fletcher-Goldfarb-Shanno (BFGS) algorithm[54] in ONETEP to test the accuracy of the force evaluation in practical applications. Calculations on an adenine-thymine DNA base pair were carried out as a first test case. This system is weakly bound by two hydrogen bonds, O···H and N···H, and therefore more sensitive to small variations of the energy and forces. We performed calculations using the PBE[53] exchange-correlation functional with 1200 eV kinetic energy cutoff. We employed one NGWF for the hydrogen atoms and four for oxygen, carbon, and nitrogen atoms, and various NGWF radii to test the convergence of the geometry optimization calculations both with uncorrected Hellmann-Feynman forces and Pulay-corrected forces. We compared the resulting structures with those given by NWCHEM with a cc-pVTZ Gaussian basis set and CASTEP with the same kinetic energy cutoff and pseudopotentials. The results are shown in Table I.

The addition of Pulay corrections to the Hellmann-Feynman forces improves the convergence of the BFGS algorithm for all the range of NGWF radii. It has a more important effect for small localization regions, allowing relaxation of the structure to tighter tolerance thresholds. The calculations using uncorrected Hellmann-Feynman forces with small NGWF radii result in a poor description of hydrogen bonding

TABLE I. Geometry optimization of adenine-thymine using ONETEP for different localization radii R_α with HF forces and PC forces. Results show the hydrogen bond lengths, the maximum absolute value of the force, $|F|_{\max}$, and the number of BFGS steps required.

		O···H bond (Å)		N···H bond (Å)		$\|F\|_{\max}$ (eV/Å)		BFGS steps	
	R_α (Å)	HF	PC	HF	PC	HF	PC	HF	PC
ONETEP	3.70	9.77	1.73	10.64	1.60	1.028	0.010	203	222
	4.23	5.39	1.75	7.15	1.62	1.542	0.015	128	73
	4.86	1.90	1.80	1.65	1.65	1.542	0.015	80	73
	5.39	1.61	1.83	1.62	1.69	0.514	0.015	95	90
	5.82	1.73	1.83	1.64	1.71	1.028	0.015	100	63
	6.45	1.75	1.83	1.57	1.72	0.463	0.015	92	63
	6.98	1.85	1.84	1.62	1.72	0.463	0.015	97	65
	7.41	1.81	1.84	1.68	1.73	0.206	0.015	92	74
	7.94	1.83	1.84	1.67	1.73	0.051	0.015	78	69
NWCHEM	···	1.84		1.73		0.026		102	
CASTEP	···	1.85		1.75		0.010		88	

in the adenine-thymine complex, leading to heavily distorted geometry and unphysical configurations. In the uncorrected case, increasing the NGWF radius eventually results in a bound and symmetric system, although the maximum value of the residual force remains higher than in the corrected case after a similar number of BFGS steps. The convergence of the maximum element of the force is plotted in Fig. 3, which demonstrates that accuracy in the forces is crucial to achieving efficient geometry relaxation using the BFGS method. Our results also show that the converged geometry of the adenine-thymine complex obtained with Pulay-corrected forces is still sensitive to changes in the NGWF radius. Using small NGWF localization results in overbinding of the hydrogen bonds. As the NGWF radius increases, the geometry converges to the optimized structures obtained with NWCHEM and CASTEP.

We have used the relaxed structures (obtained both with uncorrected and corrected forces) to calculate the binding energy of the adenine-thymine complex, defined as $E_{\text{complex}} - E_{\text{adenine}} - E_{\text{thymine}}$. The first term corresponds to the energy of the geometry-optimized complex, and the last two are the energies of the isolated adenine and thymine molecules, respectively. In each case, the individual molecules retain the same geometry as in the complex. The results, represented in Fig. 4, show that the calculations using uncorrected Hellmann-Feynman forces lead to extreme variations and erratic convergence with increasing NGWF radius. In contrast, the structures obtained with Pulay-corrected forces converge systematically with respect to the size of the localization region. In this case, the binding energies converge within 1 kcal/mol for NGWF radii larger than 5.5 Å. The convergence of these calculations is due to the simultaneous change of the basis set (as a result of increasing NGWF radii) and the change in the initial structure. To determine the convergence of the binding energies with respect to the basis set

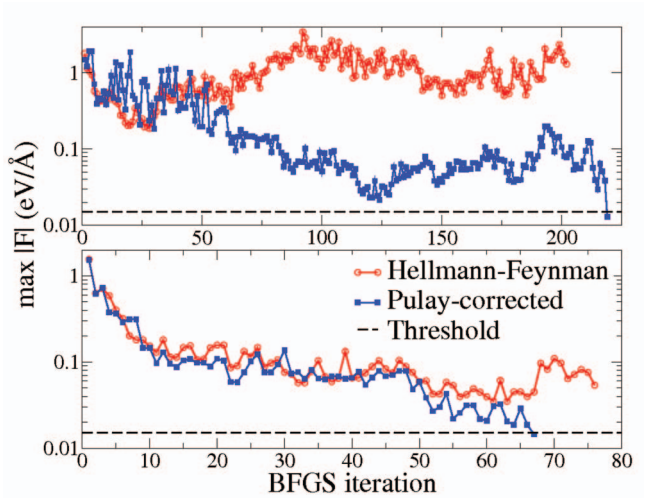

FIG. 3. Convergence of the maximum absolute value of the force during geometry optimization of the adenine-thymine DNA base pair with NGWF radii of 3.70 Å (top) and 7.94 Å (bottom). The convergence threshold was 0.015 eV/Å.

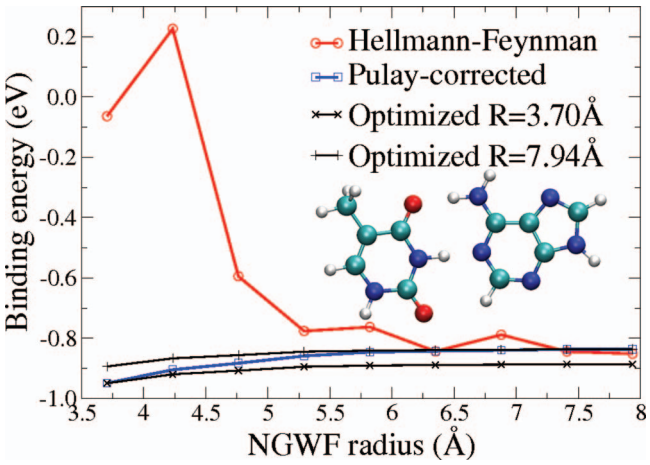

FIG. 4. Convergence of the binding energy in the adenine-thymine complex with increasing NGWF radii. The calculations that use structures obtained with Pulay-corrected forces show systematic convergence (blue squares) with increasing NGWF radius. In contrast, the calculations with structures obtained with uncorrected Hellmann-Feynman forces (red circles) lack of convergence and show large variations of the binding energy. The calculations represented with black crosses show convergence of the binding energy with increasing NGWF radius. They are based on fixed molecular geometries obtained with Pulay-corrected forces and NGWF radius of 3.70 and 7.94 Å.

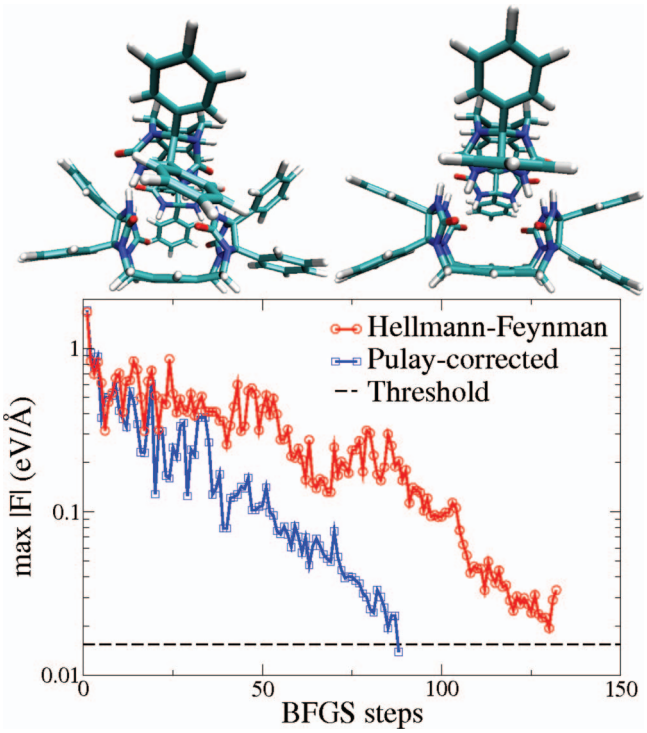

FIG. 5. Convergence of the maximum force during the BFGS geometry optimization of the tennis-ball dimer using Hellmann-Feynman forces (top left molecule) and Pulay-corrected forces (top right).

only, we chose the structures obtained with a radius of 3.70 and 7.94 Å (Pulay-corrected) and re-calculated the binding energies for different NGWF radii. In these calculations, the binding energy converges within 1 kcal/mol for NGWF radii larger than 4.2 Å. Basis set superposition error is eliminated due to the optimization of the NGWFs in terms of the psinc basis set.[55]

We have also performed geometry optimization calculations in the larger system of the "tennis-ball" self-assembling superstructure,[39,40] consisting on 176 atoms. This system is a model for protein-ligand binding interactions, formed by two identical structures that bind each other through eight hydrogen bonds when rotated 90°. We performed geometry optimization calculations using the PBE[53] functional, 1200 eV kinetic energy cutoff and one NGWF per hydrogen atom and four per oxygen, nitrogen, and carbon atoms with NGWF radius of 3.70 Å. The results, included in Fig. 5, show that calculations with uncorrected Hellmann-Feynman forces result in an asymmetric complex and in an unstable and highly oscillating minimization of the total force. On the other hand, when the Pulay corrections are taken into account, the BFGS method converges to a symmetric structure and a low threshold of force tolerance (0.015 eV/Å).

C. Geometry optimization using PAOs

We performed a number of geometry optimization calculations on the adenine-thymine DNA base pair using PAO multiple-ζ basis sets, using the same exchange-correlation functional, pseudopotentials, and kinetic energy cutoff than in the case of the NGWFs calculations discussed in Sec. IV B. The results, shown in Table II, are consistent with those obtained with NGWFs for the same radii. The calculations with the smaller basis sets tend to overbind the hydrogen bonds. Progressively larger basis sets result in structures that converge to those obtained with NGWFs, NWCHEM and CASTEP, previously shown in Table I. Basis sets of medium size such as TZP, TZDP or QZP can lead to optimum geometries.

TABLE II. Length of the two hydrogen bonds in the adenine-thymine complex obtained with different PAO multiple-ζ basis sets of different localization radius, R, given in Å. The total forces converged to 0.015 Å/eV.

	O···H bond (Å)			N···H bond (Å)		
	R = 3.70	R = 4.23	R = 4.86	R = 3.70	R = 4.23	R = 4.86
SZ	1.41	1.42	1.42	1.32	1.31	1.31
SZP	1.57	1.61	1.56	1.32	1.31	1.31
DZ	1.66	1.67	1.65	1.49	1.52	1.53
DZP	1.74	1.73	1.71	1.58	1.58	1.57
TZ	1.70	1.71	1.69	1.53	1.58	1.56
TZP	1.83	1.84	1.81	1.68	1.69	1.68
TZDP	1.79	1.84	1.79	1.68	1.68	1.68
QZ	1.73	1.71	1.71	1.55	1.56	1.57
QZP	1.81	1.82	1.81	1.67	1.66	1.69

D. Geometry optimization of large systems

As an example of the application of the aforementioned methods to large-scale systems, we performed a geometry optimization calculation on a DNA fragment of 16 base pairs consisting of 1045 atoms in vacuum. The initial structure was created using AMBER NUCGEN[56] (sequence ATCGATTGAGCTCTAG), after which we protonated the phosphate groups so that the total charge is zero. The calculations were run using the PBE exchange-correlation functional[53] and a kinetic energy cutoff of 1200 eV. We used, for each test case, NGWFs (one for hydrogen atoms, four for oxygen, nitrogen, and carbon, and nine for phosphorus), DZP and TZP PAO basis sets. The localization radius was 3.70 Å in all cases. In such large systems, achieving the same degree of convergence of the total force as we would achieve in smaller systems can be cumbersome, due to the greater number of degrees of freedom involved in the calculation. Therefore, we consider that a higher convergence threshold of 0.16 eV/Å is suitable for the purpose of demonstrating that effective structural relaxation occurs.

Figure 6 shows the convergence of the force for the different calculations, and Table III shows the optimized value of some relevant structural parameters and their change throughout the calculation. The maximum value of the force converges to the given threshold in all cases. The final structure obtained with the DZP basis set possesses clear differences with respect to those obtained with TZP and NGWFs. It displays a shorter length, a smaller radius and much shorter N···H hydrogen bonds between the base pairs. Such observations are in agreement with the results of the adenine-thymine complex discussed in Secs. IV B and IV C,

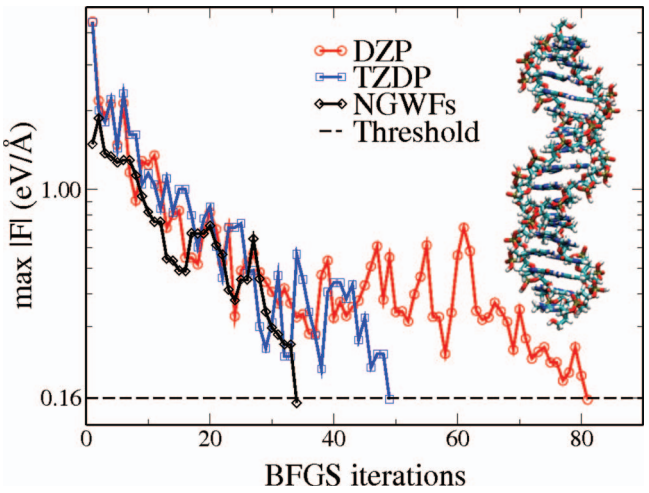

FIG. 6. Convergence of the maximum value of the force during the geometry optimization of the DNA molecule using NGWFs and DZP and TZDP PAO basis sets.

in which the DZP basis set tends to overbind hydrogen bonds compared to TDZP and NGWFs. These last two calculations, on the other hand, produce very similar results.

Noticeably, the calculation with NGWFs requires fewer BFGS steps to complete in comparison with DZP and TZDP basis sets. This is likely to be a consequence of the more accurate description of the Kohn-Sham ground state provided by the NGWF optimization. Similarly, TZDP also requires fewer BFGS steps than DZP due to its better degree of completeness. For the basis sets used in this study, each BFGS step is completed faster when using PAOs, as overall fewer matrix operations are required due to the absence of the outer loop to optimize the NGWFs. We run our calculations on 120 cores, using 15 Intel Nehalem nodes with 8 cores each. On average a BFGS step took 3.2 h with the DZP basis set, 7.6 h with TZDP basis set, and 8.3 h with the NGWFs optimized in the psinc basis set. As we can observe, the time saved per BFGS step through the use of a PAO basis set decreases as the number of basis set functions becomes larger. For this system in particular, using a DZP basis set is nearly twice as fast as the corresponding NGWF calculation, while the TDZP basis set is only marginally faster.

TABLE III. Structural parameters of the optimized 1045 atom DNA fragment as optimized by ONETEP. N···H(4), N···H(8), and N···H(12) correspond to the hydrogen bond of the fourth, eighth, and twelfth pairs, respectively, that involve a nitrogen atom.

	DZP		TZDP		NGWFs	
Basis set	Final	Change	Final	Change	Final	Change
Length (Å)	49.74	− 1.18	50.62	− 0.35	50.50	− 0.47
Diameter (Å)	15.31	0.04	15.32	0.05	15.21	− 0.06
Helix pitch (Å)	24.05	0.34	23.63	0.08	23.55	0.16
N···H(4)	1.66	− 0.21	1.78	− 0.09	1.80	− 0.07
N···H(8)	1.48	− 0.33	1.62	− 0.19	1.67	− 0.14
N···H(12)	1.54	− 0.27	1.63	− 0.18	1.64	− 0.17

V. CONCLUSIONS

We have shown that the correction to the Hellmann-Feynman forces due to the Pulay forces is essential to achieve accuracy in the total ionic forces. Using localized orbitals optimized *in situ* in terms of a basis set that is independent of the nuclear positions, such as psinc functions, does not eliminate the Pulay forces. This is due to the tendency of the kinetic energy gradient to delocalize the atomic orbitals which are constrained to be strictly localized within a sphere of finite radius. Pulay-corrected forces are consistent with the total energy after self-consistent optimization.

Geometry optimization calculations, which rely heavily upon accurate ionic forces, yield much better results when Pulay forces are taken into account. Molecular systems containing weakly bound components are better described by the inclusion of Pulay forces. Our method can be used for large-scale geometry optimization calculations on systems of more than a thousand atoms. The results converge systematically with respect to the basis set.

The corrections due to the Pulay forces also allow calculations in which the localized orbitals are fixed during the calculation to PAO. PAOs are a reliable and improvable method to construct suitable multiple-ζ basis sets of increasing accuracy. Faster geometry optimization steps are possible with PAO basis sets of medium size.

ACKNOWLEDGMENTS

A.R.S. acknowledges the support of the Engineering and Physical Sciences Research Consul (U.K.) (EPSRC (GB)) (Grant No. EP/F038038/1) for a high end computing studentship through the UK Car-Parrinello consortium. N.D.M.H. acknowledges the support EPSRC (Grant No. EP/G05567X/1) for postdoctoral funding through the HPC software development call 2008/2009. C.-K.S. acknowledges support from the Royal Society in the form of a University Research Fellowship. The authors are grateful for the computing resources provided by Southampton University's iSolutions unit (Iridis3 supercomputer) which have enabled all the calculations presented here.

APPENDIX: PSEUDOATOMIC SOLVER

1. Generating valence PAOs

Initial NGWFs can be generated by performing a Kohn-Sham DFT calculation for a pseudoatom. The pseudopotential of a single isolated ion provides the external potential, and the single-electron Kohn-Sham states are solved self-consistently at fixed occupancies. The resulting states form an ideal pseudoatomic orbital basis for calculations on molecules or solids with the same choice of pseudopotential and functional.

The PAOs are solutions of the Kohn-Sham equation,

$$\left(-\frac{1}{2}\nabla^2 + V_{\text{loc}}(r) + \hat{V}_{\text{nl}}\right)|\psi_{nlm}\rangle = \epsilon_{nl}|\psi_{nlm}\rangle, \qquad \text{(A1)}$$

where the Hamiltonian contains kinetic, local effective potential and nonlocal potential contributions for an isolated atom in spherical confinement.

The solutions to this spherically symmetric problem comprise real spherical harmonics $Z_{lm}(\theta, \varphi)$ multiplying a radial part described by a basis of normalized spherical Bessel functions $B_{l,\nu}(r)$ of given angular momentum l. This choice has been made in other implementations of similar methods.[29–31] The basis functions are defined by

$$B_{l,\nu}(r) = j_l(q_{l,\nu}r) \Big/ \left[\int_0^{R_c} |j_l(q_{l,\nu}r)|^2 r^2 dr\right]^{1/2}, \quad \text{(A2)}$$

with $q_{l,\nu}$ chosen such that $q_{l,\nu}R_c$ are the zeros of the spherical Bessel functions $j_l(x)$. This ensures that all the basis functions go to zero at the cutoff radius R_c, which is chosen to coincide with the NGWF cutoff R_α. Furthermore, $\int_0^{R_c} |B_{l,\nu}(r)|^2 r^2 dr = 1$ for all ν. The basis is made finite by including only functions with a kinetic energy less than a cutoff energy E_{cut}. The criterion $\frac{1}{2}q_{l,\nu}^2 < E_{\text{cut}}$ determines the largest ν for each l.

We therefore write the PAO $\psi_{nlm}(\mathbf{r})$ in terms of coefficients $c_{nl,\nu}$ for each basis function, in the form

$$\psi_{nlm}(\mathbf{r}) = \sum_\nu c_{nl,\nu} B_{l,\nu}(r) Z_{lm}(\theta, \varphi), \quad \text{(A3)}$$

with eigenvalues ϵ_{nl} and occupancies f_{nl} (which account for spin-degeneracy). The occupancies are fixed such that they obey the aufbau principle and sum to the number of valence electrons. Spherical symmetry means that the occupancies of all members of a given set of m-degenerate orbitals are equal, so we combine the $2l + 1$ degenerate states of differing m for a given nl state into one state to be solved with the sum of the occupancies of the shell. Henceforth, we will only consider the radial dependence $R_{nl}(r)$.

We define the local potential to be

$$V_{\text{loc}}(r) = V_{\text{psloc}}(r) + V_H(r) + V_{XC}(r) + V_{\text{conf}}(r), \quad \text{(A4)}$$

where the Hartree and XC terms are included in the standard way, as is an optional confining potential implemented as described in Ref. 28.

For each value of l we can define the Hamiltonian and overlap matrices

$$H^l_{\nu,\nu'} = \int_0^{R_c} B_{l,\nu}(r)[\hat{H} B_{l,\nu'}(r)] r^2 dr \quad \text{(A5)}$$

and

$$S^l_{\nu,\nu'} = \int_0^{R_c} B_{l,\nu}(r) B_{l,\nu'}(r) r^2 dr, \quad \text{(A6)}$$

and solve the secular equation

$$\mathbf{H}^l.\mathbf{c}_{nl} = \epsilon_{nl}\mathbf{S}^l.\mathbf{c}_{nl}, \quad \text{(A7)}$$

to give the coefficients $c_{nl,\nu}$ describing the orbitals. The orbitals are then evaluated on a regular radial real-space grid and used to construct the total density. Density mixing with a variable mixing parameter α is then used and the SCF cycle repeats until self-consistency is obtained. The result is deemed to be converged once the Harris-Foulkes[57,58] estimate of the total energy (the bandstructure energy) matches the total energy as determined from the density to within a tolerance of 2.7×10^{-4} eV, and the energy has stopped changing at each iteration to within a tolerance of 2.7×10^{-6} eV.

2. Generating larger basis sets

We follow the procedure described in Ref. 30 for generating larger PAO basis sets, appropriate for calculations with a fixed basis. Briefly, this works in two ways: first, the radial flexibility can be improved by splitting each of the valence orbitals into multiple zeta functions. Second, the highest l valence states can be polarized using perturbation theory, to produce orbitals for higher angular momentum values than exist in the valence states.

The former is achieved by setting fractional values N_i of the norm, known as the "splitnorms," which determine matching radii r_m which are then used to divide the function into components. The matching radius corresponding to each splitnorm is chosen such that the norm from r_m to the cutoff radius R_c is equal to the N_i. Typically, $N_1 \simeq 0.15$ is suitable for most elements. The first new function matches the tail of the original function beyond r_m, and has the form $r^l(a_{i,l} - b_{i,l}r^2)$ for $r < r_m$. The coefficients a_l and b_l are chosen to match the value and gradient at r_m. A second new function is then created by subtracting the new function from the original function and renormalizing it. This has the advantage that the second new function is zero beyond r_m and is thus shorter ranged. This procedure can then be repeated on new functions, using new matching radii determined from further splitnorms N_i, where each must be smaller than the last.

Generation of higher angular momentum functions is achieved through perturbation theory, as used extensively elsewhere.[13,51] A valence orbital R_{nl} with eigenvalue ϵ_{nl} is perturbed by an applied electric field in the z direction, $\Delta\hat{V} = \mathcal{E}z$. Perturbation theory then produces the first-order change in the wavefunction ΔR_{nl} as

$$(\hat{H} - \epsilon_{nl})\Delta R_{nl} = -(\Delta\hat{V} - \Delta\epsilon_{nl})R_{nl}. \quad \text{(A8)}$$

Since the perturbation is an odd function of z, the $\Delta\epsilon_{nl}$ term is always zero. The first-order change ΔR_{nl} only contains components with angular momenta $l + 1$ and $l - 1$, by the dipole selection rule. In most cases we already have angular momentum $l - 1$ terms in the basis, so only the $l + 1$ term is considered, and the coefficient of this term is dropped as it only affects the normalization (as does the field strength $\mathcal{E}$).

We can expand the radial part in terms of coefficients d_ν multiplying the basis functions for $l + 1$, as

$$\Delta R_{nl}(r) = \sum_\nu d_\nu B_{l+1,\nu}(r). \quad \text{(A9)}$$

Multiplying through by $B_{l+1,\nu'}(r)$ and solving the resulting matrix equation gives us

$$d_\nu = \left(H^{l+1}_{\nu\nu'} - \epsilon_{nl}S^{l+1}_{\nu\nu'}\right)^{-1} D_\nu, \quad \text{(A10)}$$

where D_ν is the overlap of the basis functions with the perturbation. After angular integration with $\Delta\hat{V} \propto -r\cos\theta$ this gives

$$D_\nu = -\int_0^{R_c} B_{l+1,\nu}\, r\, R_{nl}(r) r^2 dr. \quad \text{(A11)}$$

The resulting wavefunctions (after renormalization) approximately match the radial weight distribution of the original functions and have the same cutoff. They thus form an ideal

extension of the basis, suited to describing the response of the valence states to local electric fields.

The choices of PAO basis set we employed in this work were: SZ, with no extra functions beyond the valence orbitals, DZ where the valence states are split into two functions, DZP, where a set of polarization functions are added, as well as TZ, TZP, TZDP, QZ, and QZP, involving three and four basis functions and up to two polarization shells. SZ is generally regarded as insufficiently accurate for meaningful results, but typically DZP or above can be used for moderately accurate calculations, with TZDP and above providing a well-converged result (albeit at rather high cost).

[1] P. Hohenberg and W. Kohn, Phys. Rev. **136**, B864 (1964).
[2] W. Kohn and L. J. Sham, Phys. Rev. **140**, A1133 (1965).
[3] M. D. Segall, P. J. D. Lindan, M. J. Probert, C. J. Pickard, P. J. Hasnip, S. J. Clark, and M. C. Payne, J. Phys. Condens. Matter **14**, 2717 (2002).
[4] M. Valiev, E. Bylaska, N. Govind, K. Kowalski, T. Straatsma, H. V. Dam, D. Wang, J. Nieplocha, E. Apra, T. Windus, and W. de Jong, Comput. Phys. Commun. **181**, 1477 (2010).
[5] G. Kresse and J. Furthmüller, Phys. Rev. B **54**, 11169 (1996).
[6] G. te Velde, F. M. Bickelhaupt, E. J. Baerends, C. Fonseca Guerra, S. J. A. van Gisbergen, J. G. Snijders, and T. Ziegler, J. Comput. Chem. **22**, 931 (2001).
[7] P. Giannozzi, S. Baroni, N. Bonini, M. Calandra, R. Car, C. Cavazzoni, D. Ceresoli, G. L. Chiarotti, M. Cococcioni, I. Dabo, A. D. Corso, S. de Gironcoli, S. Fabris, G. Fratesi, R. Gebauer, U. Gerstmann, C. Gougoussis, A. Kokalj, M. Lazzeri, L. Martin-Samos, N. Marzari, F. Mauri, R. Mazzarello, S. Paolini, A. Pasquarello, L. Paulatto, C. Sbraccia, S. Scandolo, G. Sclauzero, A. P. Seitsonen, A. Smogunov, P. Umari, and R. M. Wentzcovitch, J. Phys. Condens. Matter **21**, 395502 (2009).
[8] W. Kohn, Phys. Rev. Lett. **76**, 3168 (1996).
[9] S. Goedecker, Rev. Mod. Phys. **71**, 1085 (1999).
[10] D. R. Bowler and T. Miyazaki, Rep. Prog. Phys. **75**, 036503 (2012).
[11] C.-K. Skylaris, P. D. Haynes, A. A. Mostofi, and M. C. Payne, J. Chem. Phys. **122**, 084119 (2005).
[12] M. J. Gillan, D. R. Bowler, A. S. Torralba, and T. Miyazaki, Comput. Phys. Commun. **177**, 14 (2007).
[13] J. M. Soler, E. Artacho, J. D. Gale, A. Garcia, J. Junquera, P. Ordejon, and D. Sanchez-Portal, J. Phys. Condens. Matter **14**, 2745 (2002).
[14] T. Ozaki and H. Kino, Phys. Rev. B **72**, 045121 (2005).
[15] N. D. M. Hine, P. D. Haynes, A. A. Mostofi, C. K. Skylaris, and M. C. Payne, Comput. Phys. Commun. **180**, 1041 (2009).
[16] A. Szabo and N. S. Ostlund, *Modern Quantum Chemistry. Introduction to Advanced Electronic Structure Theory* (Dover Publications, 1996).
[17] H. Hellmann, *Einführung in die Quantenchemie* (Deuticke, Leipzig, 1937).
[18] R. P. Feynman, Phys. Rev. **56**, 340 (1939).
[19] A. Hurley, Proc. R. Soc. London, Ser. A **226**, 179 (1954).
[20] M. Scheffler, J. P. Vigneron, and G. B. Bachelet, Phys. Rev. B **31**, 6541 (1985).
[21] M. Di Ventra and S. Pantelides, Phys. Rev. B **61**, 16207 (2000).
[22] P. Pulay, Mol. Phys. **17**, 197 (1969).
[23] J. Fattebert and F. Gygi, Comput. Phys. Commun. **162**, 24 (2004).
[24] E. R. Davidson and D. Feller, Chem. Rev. **86**, 681 (1986).
[25] P. Briddon and R. Jones, Phys. Status Solidi B **217**, 131 (2000).
[26] D. P. Chong, E. Van Lenthe, S. Van Gisbergen, and E. J. Baerends, J. Comput. Chem. **25**, 1030 (2004).
[27] B. Delley, J. Chem. Phys. **92**, 508 (1990).
[28] V. Blum, R. Gehrke, F. Hanke, P. Havu, V. Havu, X. Ren, K. Reuter, and M. Scheffler, Comput. Phys. Commun. **180**, 2175 (2009).
[29] O. F. Sankley and D. J. Niklewski, Phys. Rev. B **40**, 3979 (1989).
[30] E. Artacho, D. Sánchez-Portal, P. Ordejón, A. García, and J. M. Soler, Phys. Status Solidi B **215**, 809 (1999).
[31] A. S. Torralba, M. Todorovic, V. Brazdova, R. Choudhury, T. Miyazaki, M. J. Gillan, and D. R. Bowler, J. Phys. Condens. Matter **20**, 294206 (2008).
[32] M. Chen, G.-C. Guo, and L. He, J. Phys. Condens. Matter **22**, 445501 (2010).
[33] M. J. Louwerse and G. Rothenberg, Phys. Rev. B **85**, 035108 (2012).
[34] G. Lippert, J. Hutter, and M. Parrinello, Mol. Phys. **92**, 477 (1997).
[35] J. VandeVondele, M. Krack, F. Mohamed, M. Parrinello, T. Chassaing, and J. Hutter, Comput. Phys. Commun. **167**, 103 (2005).
[36] L. Fusti-Molnar and P. Pulay, J. Chem. Phys. **117**, 7827 (2002).
[37] M. A. Watson, Y. Kurashige, T. Nakajima, and K. Hirao, J. Chem. Phys. **128**, 054105 (2008).
[38] E. Hernández, M. J. Gillan, and C. M. Goringe, Phys. Rev. B **55**, 13485 (1997).
[39] N. Branda, R. Wyler, and J. Rebek, Science **263**, 1267 (1994).
[40] S. Fox, H. G. Wallnoefer, T. Fox, C. S. Tautermann, and C.-K. Skylaris, J. Chem. Theory Comput. **7**, 1102 (2011).
[41] L. Kleinman and D. M. Bylander, Phys. Rev. Lett. **48**, 1425 (1982).
[42] M. C. Payne, M. P. Teter, D. C. Allan, T. A. Arias, and J. D. Joannopoulos, Rev. Mod. Phys. **64**, 1045 (1992).
[43] C.-K. Skylaris, A. A. Mostofi, P. D. Haynes, O. Diéguez, and M. C. Payne, Phys. Rev. B **66**, 035119 (2002).
[44] C.-K. Skylaris and P. D. Haynes, J. Chem. Phys. **127**, 164712 (2007).
[45] C.-K. Skylaris, A. A. Mostofi, P. Haynes, C. J. Pickard, and M. C. Payne, Comput. Phys. Commun. **140**, 315 (2001).
[46] P. D. Haynes, C. K. Skylaris, A. A. Mostofi, and M. C. Payne, J. Phys.: Condens. Matter **20**, 294207 (2008).
[47] X. P. Li, R. W. Nunes, and D. Vanderbilt, Phys. Rev. B **47**, 10891 (1993).
[48] N. D. M. Hine, M. Robinson, P. D. Haynes, C. K. Skylaris, M. C. Payne, and A. A. Mostofi, Phys. Rev. B **83**, 195102 (2011).
[49] C.-K. Skylaris, O. Diéguez, P. D. Haynes, and M. C. Payne, Phys. Rev. B **66**, 073103 (2002).
[50] T. Miyazaki, D. R. Bowler, R. Choudhury, and M. J. Gillan, J. Chem. Phys. **121**, 6186 (2004).
[51] E. Artacho, E. Anglada, O. Dièguez, J. D. Gale, A. García, J. Junquera, R. M. Martin, P. Ordejón, J. M. Pruneda, D. Sãnchez-Portal, and J. M. Soler, J. Phys. Condens. Matter **20**, 064208 (2008).
[52] M. Tafipolsky and R. Schmid, J. Chem. Phys. **124**, 174102 (2006).
[53] J. P. Perdew, K. Burke, and M. Ernzerhof, Phys. Rev. Lett. **77**, 3865 (1996).
[54] B. G. Pfrommer, M. Cote, S. G. Louie, and M. L. Cohen, J. Comput. Phys. **131**, 233 (1997).
[55] P. D. Haynes, C.-K. Skylaris, A. A. Mostofi, and M. C. Payne, Chem. Phys. Lett. **422**, 345 (2006).
[56] D. A. Case, T. A. Darden, I. T. E. Cheatham, C. L. Simmerling, J. Wang, R. E. Duke, R. Luo, R. C. Walker, W. Zhang, K. M. Merz, B. P. Roberts, B. Wang, S. Hayik, A. Roitberg, G. Seabra, I. Kolossváry, K. F. Wong, F. Paesani, J. Vanicek, J. Liu, X. Wu, S. R. Brozell, T. Steinbrecher, H. Gohlke, Q. Cai, X. Ye, J. Wang, M.-J. Hsieh, G. Cui, D. Roe, D. H. Mathews, M. Seetin, C. Sagui, V. Babin, T. Luchko, S. Gusarov, A. Kovalenko, and P. A. Kollman, Amber 11, 2010 (University of California, San Franciso).
[57] J. Harris, Phys. Rev. B **31**, 1770 (1985).
[58] W. M. C. Foulkes and R. Haydock, Phys. Rev. B **39**, 12520 (1989).